Weak Universality Induced by $Q = \pm 2e$ Charges at the Deconfinement Transition of a (2 + 1)-Dimensional U(1) Lattice Gauge Theory

Indrajit Sau,[1] Arnab Sen,[1] and Debasish Banerjee[2,3]
[1]School of Physical Sciences, Indian Association for the Cultivation of Science, Kolkata 700032, India
[2]Theory Division, Saha Institute of Nuclear Physics, 1/AF Bidhan Nagar, Kolkata 700064, India
[3]Homi Bhabha National Institute, Training School Complex, Anushaktinagar, Mumbai 400094, India

(Received 19 October 2022; revised 30 January 2023; accepted 31 January 2023; published 17 February 2023)

Matter-free lattice gauge theories (LGTs) provide an ideal setting to understand confinement to deconfinement transitions at finite temperatures, which is typically due to the spontaneous breakdown (at large temperatures) of the center symmetry associated with the gauge group. Close to the transition, the relevant degrees of freedom (Polyakov loop) transform under these center symmetries, and the effective theory depends on only the Polyakov loop and its fluctuations. As shown first by Svetitsky and Yaffe, and subsequently verified numerically, for the U(1) LGT in $(2 + 1)$ dimensions, the transition is in the 2D XY universality class, while for the Z_2 LGT, it is in the 2D Ising universality class. We extend this classic scenario by adding higher charged matter fields and show that the critical exponents γ and ν can change continuously as a coupling is varied, while their ratio is fixed to the 2D Ising value. While such *weak universality* is well known for spin models, we demonstrate this for LGTs for the first time. Using an efficient cluster algorithm, we show that the finite temperature phase transition of the U(1) quantum link LGT in the spin $S = \frac{1}{2}$ representation is in the 2D XY universality class, as expected. On the addition of $Q = \pm 2e$ charges distributed thermally, we demonstrate the occurrence of weak universality.

DOI: 10.1103/PhysRevLett.130.071901

Introduction.—Phases of matter at extreme temperature, pressure, and density often challenge our conventional notions and stimulate extensive research, both experimentally and theoretically. Of particular relevance are the physics of the early Universe and the interior of neutron stars. Both scenarios are expected to have a microscopic description through quantum chromodynamics (QCD), a field theory of quarks and gluons [1–4]. As a strongly interacting quantum field theory (QFT), QCD confines color-charge-carrying quarks and gluons into color singlet bound states, rendering conventional perturbation techniques unsuitable.

Lattice gauge theories (LGTs) are nonperturbative formulation of QFTs, where Markov chain Monte Carlo methods are used to compute physical observables, and supply the most reliable insights about strong-interaction physics [5]. The possibility of a thermal phase transition out of the confined phase was explored first in pure gauge theories. It is universally accepted that pure SU(3) gauge theory has a first-order deconfinement phase transition [6,7], while the SU(2) gauge theory has a second-order phase transition [8,9]. For QCD with physical quark masses, there is only a crossover from the hadronic phase to the deconfined quark gluon plasma phase [10,11].

The finite temperature phase transition in pure gauge theories can be described using an effective field theory (EFT). Svetitsky and Yaffe (SY) [12] used the insight that the confinement to deconfinement transition in a pure gauge theory is due to the spontaneous breakdown of the global center symmetry of the gauge group to show that the relevant degrees of freedom in the EFT are the Polyakov loop (order parameter) and its fluctuations. Integrating out all other degrees of freedom in the original gauge theory in $(d + 1)$ dimensions, they argued that the EFT corresponds to a d-dimensional spin model. The confinement in the original gauge theory ensures that the effective couplings in the spin system are short ranged. Using universality, they argued that the original gauge theory should share the same transition as the effective spin model, if both theories have continuous phase transitions. This SY scenario has been verified in different numerical simulations [13–18] and is widely regarded as a success of universality.

In this Letter, we report an extension of the SY approach for $(2 + 1)$-dimensional U(1) lattice gauge theory in the presence of higher charges $\pm 2e$ (where e denotes the fundamental unit of charge, which we set to 1 henceforth), using the quantum link gauge theory (QLGT) formulation. QLGTs are generalizations of Wilson's LGTs which are

extensively used to investigate properties of gauge theories numerically as well as with quantum simulators [19,20]. As expected from the SY conjecture, the pure U(1) QLGT undergoes a Berezinskii-Kosterlitz-Thouless (BKT) deconfinement transition. Introduction of thermally generated ± 2 charges breaks the U(1) global center symmetry to a Z_2 center symmetry and, thus, predicts a deconfinement transition with 2D Z_2 critical exponents if the transition is continuous. Instead, we demonstrate a continuous transition with weak universality [21], characterized by large values of critical exponents like γ, ν, and β, while others like η and δ defined directly at the critical point, as well as the ratios of the critical exponents are fixed to the 2D Z_2 Ising model. Weak universality has been observed in a variety of systems [22–30], however; we demonstrate this at the deconfinement transition of a LGT for the first time and extend the SY conjecture to include this possibility. We perform extensive finite size scaling (FSS) studies on lattices up to $(512a)^2$ (a denotes the lattice spacing) with very small Trotter steps $\epsilon/J \sim 0.05$ (J denotes a microscopic coupling) to demonstrate the BKT as well as the weak universality scenario at the deconfinement transition in the absence and presence of the ± 2 charges, respectively.

Model, simulations, and phase diagram.—The QLGTs we consider use quantum spin $S = \frac{1}{2}$ to represent gauge fields on the links $(x, \hat{\mu})$ of a square lattice. The electric flux operator $E_{x,\hat{\mu}} = S^3_{x,\hat{\mu}}$ takes two values $\pm\frac{1}{2}$, while the gauge fields are the raising (lowering) operators of electric flux: $U^{(\dagger)}_{x,\hat{\mu}} = S^{+(-)}_{x,\hat{\mu}}$. The Hamiltonian operator is the sum of elementary plaquette terms:

$$H = -J\sum_{\square}[(U_{\square} + U^{\dagger}_{\square}) - \lambda(U_{\square} + U^{\dagger}_{\square})^2], \qquad (1)$$

where $U_{\square} = U_{x,\hat{\mu}}U_{x+\hat{\mu},\hat{\nu}}U^{\dagger}_{x+\hat{\nu},\hat{\mu}}U^{\dagger}_{x,\hat{\nu}}$. We set both the lattice spacing and J to 1 henceforth. Figure 1(a) shows the setup of the lattice. The electric fluxes are shown as directed arrows. We note that $U_{\square}(U^{\dagger}_{\square})$ reverses the orientation of the electric flux around the plaquette (clockwise to anticlockwise and vice versa), while all nonflippable plaquettes are annihilated. The λ term is akin to a potential energy, counting the total number of flippable plaquettes. The U(1) gauge symmetry is generated by the Gauss law operator $G_x = \sum_{\hat{\mu}}(E_{x,\hat{\mu}} - E_{x-\hat{\mu},\hat{\mu}})$ and commutes with the Hamiltonian: $[G_x, H] = 0$. The physical states in the vacuum sector satisfy $G_x|\psi\rangle = 0$ (six allowed states for each vertex of the square lattice) for all sites x. The presence of $Q = \pm 2$ extends the Gauss law to also include $G_x|\phi\rangle = \pm 2|\phi\rangle$. Imposing periodic boundary conditions, only states with zero total charge are allowed. Figure 1(b) shows all the allowed configurations (six with $Q_x = 0$, one each with $Q_x = 2$ and $Q_x = -2$) in our model (with equal weights). A detailed discussion about the symmetries is given in Supplemental Material (Sec. A) [31]. At finite temperature $T = 1/\beta$, the equilibrium properties can be obtained from the partition function $Z = \mathrm{Tr}[e^{-\beta H}\mathbb{P}_G]$, where $\mathbb{P}_G = \prod_x \frac{1}{8}\{6\delta(G_x) + \delta(G_x - 2) + \delta(G_x + 2)\}$ is the projection to Gauss' law allowed states.

While the charges $Q = \pm 2$ do not have a kinetic energy term in the Hamiltonian, they are generated and become mobile due to thermal fluctuations. The $Q = \pm 2$ charges can be regarded as an example of *annealed disorder* [32], where these *impurities* are in thermal equilibrium with the rest of the system. As is expected of a confining theory, at $T = 0$, the charges are high-energy states and, thus, do not appear. However, close to the deconfinement phase transition (when $T \sim \lambda J \sim M$, where M is the rest mass of the charges), the charges are thermally generated and affect the critical properties of the system as we demonstrate later. In Supplemental Material (Sec. A) [31], we show how the presence of $Q = \pm 2$ charges gives rise to an effective Z_2 Gauss' law for the theory.

In Fig. 2, we sketch a finite temperature phase diagram of the model with and without the charges. The quantum

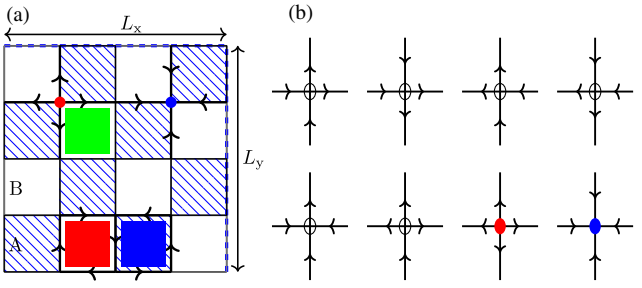

FIG. 1. (a) Sketch of the lattice—the dashed and clear plaquettes denote the A and B sublattice, respectively. $Q = \pm 2e$ charges are shown as red and blue circles, respectively. Plaquettes can be nonflippable (shaded in green), especially when it has a charge $\pm 2e$ at a corner, or flippable in the clockwise (red) or anticlockwise (blue) sense. (b) The different Gauss law realizations: The first six have $Q = 0$, while the last two have $Q = \pm 2e$ at the vertex.

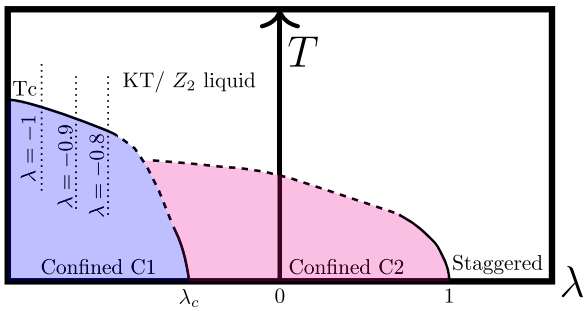

FIG. 2. The $T - \lambda$ phase diagram: At $T = 0$, there are two confined phases ($C1$ and $C2$) separated by a weak first-order phase transition. Beyond $\lambda = 1$, the staggered phase is encountered. At high T, there is a pure U(1) liquid, or a Z_2 liquid where $Q = \pm 2$ charges exist. We study the finite temperature phase diagram here. The dashed lines indicate possible phase boundaries.

phase transition in λ (at $T = 0$) revealed two distinct crystalline confined phases ($C1$ and $C2$) separated by a weak first-order phase transition at $\lambda_c \sim -0.36$ [33,34]. The phases can be understood via a two-component magnetization [measured, respectively, on sublattice A and B; see Fig. 1(a)]. In phase $C1$ both sublattices order (spontaneously breaking the lattice translation and charge conjugation), while for phase $C2$ only one of the sublattices order (breaking lattice translations). On raising the temperature, these symmetries are restored accompanied with the spontaneous breakdown of the U(1) global center symmetry, and SY analysis suggests a BKT phase transition. With the charges $Q = \pm 2$ in the ensemble, the quantum phase transition remains unchanged, while the thermal transition is modified. The charges break the U(1) center symmetry to a Z_2 subgroup, leading one to naively expect a continuous transition with 2D Z_2 critical exponents. However, the thermal transition now displays properties associated with weak universality. We concentrate on a region of λ away from λ_c such that our results are not influenced by the properties near the quantum phase transition.

We study the model using a cluster quantum Monte Carlo (QMC) algorithm, applied to the (Kramers-Wannier) dualized version of the model [35] on a lattice with L (L_T) number of points in the spatial (temporal) direction. The dualized model comprises of the height variables $h^{A,B}$ at the center of the A and B sublattices (see Fig. 1) and can be mapped to the fluxes $E_{x,\hat{\mu}}$. The algorithm builds clusters on $h^{A,B}$, which are then flipped and update the $E_{x,\hat{\mu}}$ efficiently. A comparison of the QMC results (working with $h^{A,B}$), in both the absence and presence of $Q = \pm 2$ charges, with exact diagonalization results (working with $E_{x,\hat{\mu}}$) on small lattices is shown in Supplemental Material (Sec. C) [31]. Working in the Hamiltonian approach, it is nontrivial to measure the Polyakov loop directly. Instead, we consider the sublattice magnetizations

$$M_X = \frac{1}{L_T}\sum_{\tilde{x}} \eta^X_{\tilde{x}} h^X_{\tilde{x}}, \quad \text{where } X = A, B \tag{2}$$

and $\tilde{x}$ denotes the dual sites. The phase factors $\eta^X_{\tilde{x}}$ capture the ordering of the h^X corresponding to the flippability of the plaquettes. In Supplemental Material (Sec. B) [31], we show that (M_A, M_B) serve as order parameters for the deconfinement transition. For FSS studies, we use total and connected susceptibilities:

$$\chi_{\text{tot}} = \frac{1}{V}\langle M^2\rangle, \qquad \chi_{\text{conn}} = \frac{\beta}{V}\sum_X (\langle M_X^2\rangle - \langle |M_X|\rangle^2), \tag{3}$$

where $M^2 = \sum_{X=A,B}(M_X^2)$, $V = L^2$, and $\beta = \epsilon L_T$. Three different Binder cumulants were also used to estimate the critical exponents:

$$Q_1 = \frac{1}{2}\sum_X \frac{\langle |M_X|\rangle^2}{\langle M_X^2\rangle}; \qquad Q_{2a} = 2 - \frac{\langle M^4\rangle}{\langle M^2\rangle^2};$$
$$Q_{2b} = \frac{3}{2} - \frac{1}{4}\sum_X \frac{\langle M_X^4\rangle}{\langle M_X^2\rangle^2}. \tag{4}$$

Finite temperature transition and FSS.—The FSS hypothesis for the order parameter predicts that the Binder cumulants are universal at the critical point [36–38]. We use this feature to show that the theory with and without the charges has different thermal behavior. In the left panel in Fig. 3 [the pure U(1) theory], the Binder Q_1 curves for different lattice sizes L collapse on each other at high T, while they differ in the low-T phase. This is the expected behavior for an XY universality, where a critical phase goes into a massive phase through the BKT transition. The right panel shows Q_1 for the U(1) theory with charges $Q = \pm 2$ for different L, which cross each other at $\beta_c \approx 0.815$. We will postpone a detailed study of the BKT phase transition to a future publication [39], since it establishes the conventional wisdom, and concentrate here solely on the other transition.

We extract the critical temperature $T_c = 1/\beta_c$ from crossing points of the curves of three different observables ($\chi_{\text{tot}} L^{-\gamma/\nu}$, Q_1, and Q_{2a}). Figure 4 (top panel) shows $\chi_{\text{tot}} L^{-\gamma/\nu}$ vs β for $L = 64, \ldots, 512$ and $L_T = 24$. In this analysis, we fixed $\gamma/\nu = 7/4$, the value for 2D, Z_2 universality class. We will derive this independently later, and fitting for the ratio γ/ν only increases the uncertainties without any gain. Moreover, we need very precise estimates of β_c to compute ν. Using a second-order polynomial interpolation to extract the crossing points of lattices $(L, 2L)$, we observe a surprisingly flat behavior for

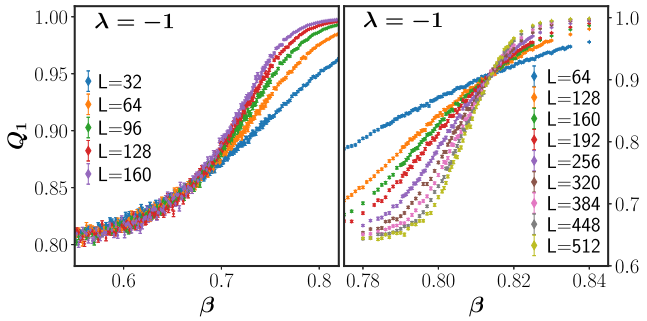

FIG. 3. The Binder cumulant Q_1 for the U(1) QLGT without (left) and with (right) the charges $Q = \pm 2$. The former displays a 2D XY scenario (critical high-T and gapped low-T phase), while the latter exhibits a 2D Ising scenario (gapped high-T and low-T) phases as one would expect from the SY analysis. We demonstrate weak universality for the latter case.

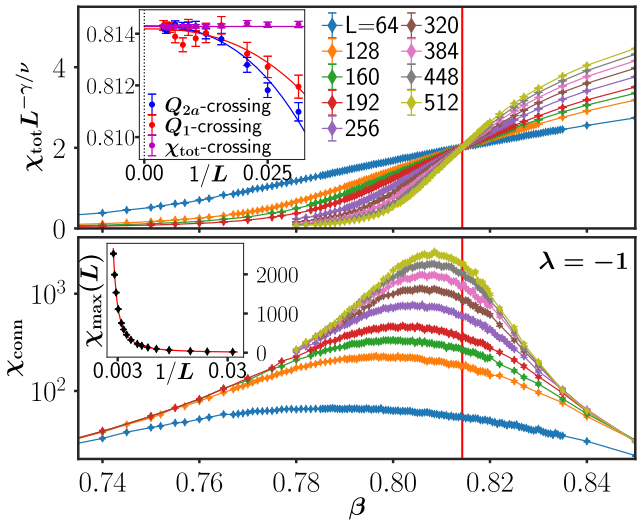

FIG. 4. Top: The critical temperature β_c of the theory with charges is estimated by the crossing of $\chi_{\rm tot}$ for different L. Inset: Estimates of β_c using Q_1 and Q_{2a} yield consistent results. Bottom: Plot of $\chi_{\rm conn}$ vs β for various L shows a peak, whose scaling with L (inset) is used to extract γ/ν. The vertical line denotes β_c.

estimates of $\beta_c(L)$ from $\chi_{\rm tot}$ as a function of $1/L$, as shown in the inset. Estimates of β_c were also extracted from the crossing points of Q_1 and Q_{2a} curves. As shown in the inset, those estimates have larger finite size corrections but yield the same β_c for $L > 100$. Therefore, we quote the value of $\beta_c(L \to \infty, L_T = 24)$ by fitting a constant to the β_c estimates from $\chi_{\rm tot}$ and report it in Table I for different L_T values and three different $\lambda = -1.0, -0.9, -0.8$ values.

We turn to the estimate of the critical exponents. The scaling of the peak of $\chi_{\rm conn}$, $\chi_{\rm conn,max}(L) = bL^{\gamma/\nu} = bL^{2-\eta}$ can be reliably used to extract η (and, thus, also γ/ν). This quantity is shown (in a semilog scale) in Fig. 4 (bottom panel) vs β, with the vertical line indicating β_c in the thermodynamic limit. The inset shows a power law fit to the $1/L$ dependence of $\chi_{\rm conn}$, from which η is extracted and reported for all our lattices and λ values in Table I.

TABLE I. Estimates of β_c, η, and ν for different values of L_T and λ.

L_T	β_c	η	$\nu(Q_1)$	$\nu(Q_{2a})$	$\nu(Q_{2b})$
		$\lambda = -1.0$			
24	0.814 279(14)	0.2472(9)	1.35(2)	1.38(1)	1.38(2)
16	0.813 783(15)	0.2479(9)	1.32(4)	1.34(2)	1.34(4)
8	0.811 129(14)	0.2489(8)	1.33(3)	1.31(2)	1.34(3)
4	0.801 059(12)	0.2509(8)	1.29(1)	1.31(1)	1.29(2)
2	0.767 685(10)	0.2497(7)	1.19(1)	1.20(1)	1.20(1)
		$\lambda = -0.9$			
24	0.885 292(17)	0.2550 (18)	1.45(3)	1.47(4)	1.45(3)
		$\lambda = -0.8$			
24	0.968 196(26)	0.2511 (10)	1.64(9)	1.68(4)	1.64(8)

Our numerical estimates of η for different L_T and λ are consistent with the 2D Z_2 universality class. The largest deviation is only at the 3σ level for $L_T = 24$ and $\lambda = -1$, while most values are consistent with $\eta = \frac{1}{4}$ within 1σ. Moreover, this is also consistent with weak universality, where deviation from the critical exponent ratios is not observed.

Weak universality.—The next step to substantiate our claim involves the accurate computation of ν independently, for which we use all three Binder ratios. We employ the well-known result [38,40] that for a dimensionless phenomenological coupling $R(\beta, L)$, the slope at β_c directly yields the exponent ν, $[\partial R(L)/\partial\beta]|_{\beta_c} = aL^{1/\nu}(1 + bL^{-\omega})$. For large lattices (or for large ω), plotting the derivative (at β_c) vs L in a log-log scale enables us to compute $1/\nu$ from the slope. The crucial requirement here is the very precise estimate of β_c, which we have already described. Performing this analysis using all three Binder ratios gives us consistent estimates of ν. The particular analysis for Q_{2a} for $L_T = 24$ and three different $\lambda = -1.0, -0.9, -0.8$ is shown in Fig. 5. To obtain the derivatives, we first fit the Binder ratios around β_c to second-order polynomials and then take the derivative analytically with respect to β. Note that since the Binder ratios are all O(1) numbers and have a smooth behavior around β_c, the polynomial fit is free of any systematic errors. Statistical errors are computed using bootstrapping samples from the entire dataset. While the data are sufficiently accurate to extract reliable estimates of ν, we are unable to estimate ω reliably. However, it is clear from the figure that the slopes of the curve (horizontally and vertically displaced for better visibility) are

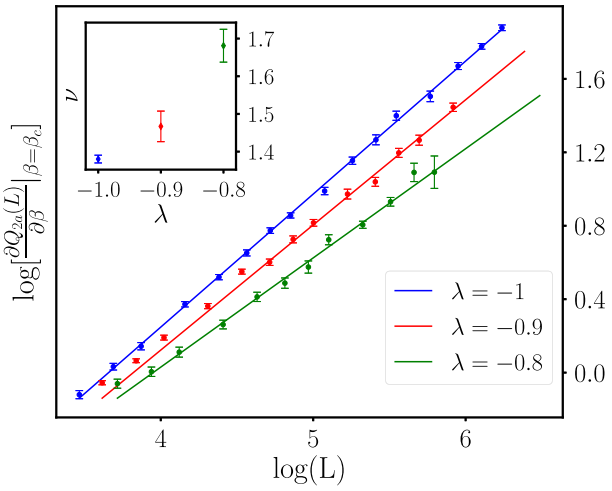

FIG. 5. Extraction of ν from the slope of derivative of Q_{2a} at β_c. The fits were done for $L = 32, \ldots, 512$ for $\lambda = -1$, $L = 96, \ldots, 320$ for $\lambda = -0.9$, and $L = 40, \ldots, 320$ for $\lambda = -0.8$. The three curves correspond to different λ which are vertically and horizontally displaced for better visibility. The inset shows the change of ν with λ.

significantly different from the 2D Z_2 universality class value of $\nu = 1$. Instead, we witness significantly large values of ν as extracted from the coupling Q_{2a}: 1.38(1) for $\lambda = -1.0$, 1.47(4) for $\lambda = -0.9$, and 1.68(4) for $\lambda = -0.9$. These values are collected in Table I, along with the corresponding estimates from the Q_1 and Q_{2b}. We note that all three estimates of ν at a fixed λ agree with each other and increase monotonically with λ. In particular, the inset in Fig. 5 displays this variation clearly. Not only are these values of ν anomalously large, but they also vary smoothly with the microscopic coupling. Both these features are hallmarks of weak universality.

An intriguing question is the reason for the occurrence of weak universality. According to the theory of renormalization group, a marginal operator [32,41,42] is needed to generate a line of fixed points with continuously varying critical exponents. In Supplemental Material (Sec. D) [31], we show the behavior of $\langle Q^2 \rangle$ (normalized with the volume) as a function of β at $\lambda = -1, -0.9, -0.8$. A small yet nonzero ($\langle Q^2 \rangle \approx 0.03$, where $\langle Q^2 \rangle_{\max} = 1$ as $T \to \infty$) critical density of charges in the vicinity of β_c suggests that charged operators play a nontrivial role in deciding such an operator.

Conclusions and outlook.—In this Letter, we demonstrated that the presence of charges can give rise to the phenomenon of weak universality at the thermal phase transition in a pure gauge theory, using the example of a $(2+1)$-dimensional U(1) QLGT. The Binder cumulant across the phase transition (Fig. 3) illustrates the difference. Using $\chi_{\text{tot}}(L)$ and the Binder ratios, we located β_c very accurately and then used the scaling of $\chi_{\text{conn,max}}(L)$ to compute η, which is compatible with the 2D Z_2 value, as expected from universality arguments. Finally, using three Binder ratios, we demonstrate that the individual exponents ν (and γ) have anomalously large values compared to the 2D Z_2 value and vary smoothly as a function of the microscopic coupling λ. These three pieces of evidence conclusively show that weak universality is relevant for this thermal transition instead of the usual universality scenario.

Our results open some very intriguing directions for further research. A close examination of the charge and the electric flux distribution at β_c could provide a better understanding of a possible marginal operator, which can be included in an effective field theory description [39]. It is also interesting to follow the thermal transition to more negative values of λ to explore whether it reaches the 2D Z_2 limit. Finally, exploring the phase diagram where three phases ($C1$, $C2$, and KT or Z_2 liquid) meet is an exciting project for the future. The prospect that this model could be realized in near-term quantum simulator setups makes these results potentially interesting [43,44]. Whether such weak universality occurs for other gauge theories is an open question.

We thank Shailesh Chandrasekharan and Uwe-Jens Wiese for useful discussions. We acknowledge the computational resources provided by IACS and SINP. D. B. acknowledges assistance from SERB Starting Grant No. SRG/2021/000396-C from the DST (Government of India).

[1] Frank Wilczek, QCD in extreme conditions, *9th CRM Summer School: Theoretical Physics at the End of the 20th Century* (1999), pp. 567–636, arXiv:hep-ph/0003183.
[2] Owe Philipsen, Constraining the phase diagram of QCD at finite temperature and density, Proc. Sci. LATTICE2019 (**2019**) 273 [arXiv:1912.04827].
[3] Massimo D'Elia, High-temperature QCD: Theory overview, Nucl. Phys. **A982**, 99 (2019).
[4] Sayantan Sharma, Recent theoretical developments on QCD matter at finite temperature and density, Int. J. Mod. Phys. E **30**, 2130003 (2021).
[5] Andreas S. Kronfeld *et al.* (USQCD Collaboration), Lattice QCD and particle physics, arXiv:2207.07641.
[6] Michael Creutz and K. J. M. Moriarty, Numerical Studies of Wilson loops in SU(3) gauge theory in four-dimensions, Phys. Rev. D **26**, 2166 (1982).
[7] John B. Kogut, J. Polonyi, H. W. Wyld, J. Shigemitsu, and D. K. Sinclair, Further evidence for the first order nature of the pure gauge SU(3) deconfinement transition, Nucl. Phys. **B251**, 311 (1985).
[8] M. Creutz, Monte Carlo Study of quantized SU(2) gauge theory, Phys. Rev. D **21**, 2308 (1980).
[9] R. V. Gavai, The deconfinement transition in SU(2) lattice gauge theories, Nucl. Phys. **B215**, 458 (1983).
[10] P. Hasenfratz, F. Karsch, and I. O. Stamatescu, The SU(3) deconfinement phase transition in the presence of quarks, Phys. Lett. **133B**, 221 (1983).
[11] Tanmoy Bhattacharya, M. I. Buchoff, N. H. Christ, H. T. Ding, R. Gupta *et al.*, QCD Phase Transition with Chiral Quarks and Physical Quark Masses, Phys. Rev. Lett. **113**, 082001 (2014).
[12] Benjamin Svetitsky and Laurence G. Yaffe, Critical behavior at finite-temperature confinement transitions, Nucl. Phys. **B210**, 423 (1982).
[13] M. Caselle and M. Hasenbusch, Deconfinement transition and dimensional crossover in the 3-D gauge Ising model, Nucl. Phys. **B470**, 435 (1996).
[14] Claudio Bonati and Massimo D'Elia, Phase diagram of the 4D U(1) model at finite temperature, Phys. Rev. D **88**, 065025 (2013).
[15] Richard Lau and Michael Teper, The deconfining phase transition of SO(N) gauge theories in $2+1$ dimensions, J. High Energy Phys. 03 (2016) 072.
[16] Oleg Borisenko, Volodymyr Chelnokov, Francesca Cuteri, and Alessandro Papa, Berezinskii-Kosterlitz-Thouless phase transitions in two-dimensional non-Abelian spin models, Phys. Rev. E **94**, 012108 (2016).
[17] Minati Biswal, Mridupawan Deka, Sanatan Digal, and P. S. Saumia, Confinement-deconfinement transition in SU(2) Higgs theory, Phys. Rev. D **96**, 014503 (2017).

[18] Yoshinobu Kuramashi and Yusuke Yoshimura, Three-dimensional finite temperature Z_2 gauge theory with tensor network scheme, J. High Energy Phys. 08 (2019) 023.
[19] Uwe-Jens Wiese, Ultracold quantum gases and lattice systems: Quantum simulation of lattice gauge theories, Ann. Phys. (Berlin) **525**, 777 (2013).
[20] Uwe-Jens Wiese, From quantum link models to D-theory: A resource efficient framework for the quantum simulation and computation of gauge theories, Phil. Trans. R. Soc. A **380**, 20210068 (2021).
[21] M. Suzuki, New universality of critical exponents, Prog. Theor. Phys. **51**, 1992 (1974).
[22] R. J. Baxter, Eight-Vertex Model in Lattice Statistics, Phys. Rev. Lett. **26**, 832 (1971).
[23] J. Ashkin and E. Teller, Statistics of two-dimensional lattices with four components, Phys. Rev. **64**, 178 (1943).
[24] P. A. Pearce and D. Kim, Continuously varying exponents in magnetic hard squares, J. Phys. A **20**, 6471 (1987).
[25] Fabien Alet, Jesper Lykke Jacobsen, Grégoire Misguich, Vincent Pasquier, Frédéric Mila, and Matthias Troyer, Interacting Classical Dimers on the Square Lattice, Phys. Rev. Lett. **94**, 235702 (2005).
[26] A. Malakis, A. N. Berker, I. A. Hadjiagapiou, and N. G. Fytas, Strong violation of critical phenomena universality: Wang-Landau study of the two-dimensional Blume-Capel model under bond randomness, Phys. Rev. E **79**, 011125 (2009).
[27] S. L. A. de Queiroz, Scaling behavior of a square-lattice Ising model with competing interactions in a uniform field, Phys. Rev. E **84**, 031132 (2011).
[28] Songbo Jin, Arnab Sen, and Anders W. Sandvik, Ashkin-Teller Criticality and Pseudo-First-Order Behavior in a Frustrated Ising Model on the Square Lattice, Phys. Rev. Lett. **108**, 045702 (2012).
[29] Songbo Jin, Arnab Sen, Wenan Guo, and Anders W. Sandvik, Phase transitions in the frustrated Ising model on the square lattice, Phys. Rev. B **87**, 144406 (2013).
[30] Takafumi Suzuki, Kenji Harada, Haruhiko Matsuo, Synge Todo, and Naoki Kawashima, Thermal phase transition of generalized Heisenberg models for SU (N) spins on square and Honeycomb lattices, Phys. Rev. B **91**, 094414 (2015).
[31] See Supplemental Material at http://link.aps.org/supplemental/10.1103/PhysRevLett.130.071901 for symmetries of the model, details of the cluster algorithm, order parameters, comparison of exact diagonalization and cluster algorithm data, and behavior of local charge density with temperature.
[32] John Cardy, *Scaling and Renormalization in Statistical Physics*, Cambridge Lecture Notes in Physics (Cambridge University Press, Cambridge, England, 1996).
[33] D. Banerjee, F. J. Jiang, P. Widmer, and U. J. Wiese, The $(2+1)$-d U(1) quantum link model masquerading as deconfined criticality, J. Stat. Mech. (2013) P12010.
[34] Ferdinand Tschirsich, Simone Montangero, and Marcello Dalmonte, Phase diagram and conformal string excitations of square ice using gauge invariant matrix product states, SciPost Phys. **6**, 028 (2019).
[35] Debasish Banerjee, Recent progress on cluster and meron algorithms for strongly correlated systems, Indian J. Phys. A **95**, 1669 (2021).
[36] K. Binder, Monte Carlo calculation of the surface tension for two- and three-dimensional lattice-gas models, Phys. Rev. A **25**, 1699 (1982).
[37] K. S. D. Beach, Ling Wang, and Anders W. Sandvik, Data collapse in the critical region using finite-size scaling with subleading corrections, arXiv:cond-mat/0505194.
[38] Ling Wang, K. S. D. Beach, and Anders W. Sandvik, High-precision finite-size scaling analysis of the quantum-critical point of $s = 1/2$ Heisenberg antiferromagnetic bilayers, Phys. Rev. B **73**, 014431 (2006).
[39] Sau *et al.* (to be published).
[40] Martin Hasenbusch, Finite size scaling study of lattice models in the three-dimensional Ising universality class, Phys. Rev. B **82**, 174433 (2010).
[41] Jorge V. José, Leo P. Kadanoff, Scott Kirkpatrick, and David R. Nelson, Renormalization, vortices, and symmetry-breaking perturbations in the two-dimensional planar model, Phys. Rev. B **16**, 1217 (1977).
[42] Gesualdo Delfino and Noel Lamsen, Critical points of coupled vector-Ising systems. Exact results, J. Phys. A **52**, 35LT02 (2019).
[43] D. Marcos, P. Widmer, E. Rico, M. Hafezi, P. Rabl, U. J. Wiese, and P. Zoller, Two-dimensional lattice gauge theories with superconducting quantum circuits, Ann. Phys. (Amsterdam) **351**, 634 (2014).
[44] Alessio Celi, Benoît Vermersch, Oscar Viyuela, Hannes Pichler, Mikhail D. Lukin, and Peter Zoller, Emerging Two-Dimensional Gauge Theories in Rydberg Configurable Arrays, Phys. Rev. X **10**, 021057 (2020).